Influence of the Chemical Pressure on the Magnetic Properties of the Mixed Anion Cuprates Cu2OX2 (X = Cl, Br, I)

W. Lafargue-Dit-Hauret, X. Rocquefelte

computation

MDPI

Article

Influence of the Chemical Pressure on the Magnetic Properties of the Mixed Anion Cuprates Cu_2OX_2 (X = Cl, Br, I)

William Lafargue-Dit-Hauret *,†,‡ **and Xavier Rocquefelte** *,‡

Univ Rennes, CNRS, ISCR (Institut des Sciences Chimiques de Rennes) UMR 6226, F-35000 Rennes, France

* Correspondence: william.lafargue-dit-hauret@univ-pau.fr (W.L.-D.-H.); xavier.rocquefelte@univ-rennes1.fr (X.R.)

† Current address: Universite de Pau et des Pays de l'Adour, E2S UPPA, CNRS, IPREM, F-64053 Pau, France.

‡ These authors contributed equally to this work.

Abstract: In this study, we theoretically investigate the structural, electronic and magnetic properties of the Cu_2OX_2 (X = Cl, Br, I) compounds. Previous studies reported potential spin-driven ferroelectricity in Cu_2OCl_2, originating from a non-collinear magnetic phase existing below T_N ~70 K. However, the nature of this low-temperature magnetic phase is still under debate. Here, we focus on the calculation of *J* exchange couplings and enhance knowledge in the field by (i) characterizing the low-temperature magnetic order for Cu_2OCl_2 and (ii) evaluating the impact of the chemical pressure on the magnetic interactions, which leads us to consider the two new phases Cu_2OBr_2 and Cu_2OI_2. Our *ab initio* simulations notably demonstrate the coexistence of strong antiferromagnetic and ferromagnetic interactions, leading to spin frustration. The T_N Néel temperatures were estimated on the basis of a quasi-1D AFM model using the *ab initio* *J* couplings. It nicely reproduces the T_N value for Cu_2OCl_2 and allows us to predict an increase of T_N under chemical pressure, with $T_N = 120$ K for the dynamically stable phase Cu_2OBr_2. This investigation suggests that chemical pressure is an effective key factor to open the door of room-temperature multiferroicity.

Keywords: Cu_2OCl_2; Cu_2OBr_2; Cu_2OI_2; oxyhalides; density functional theory; magnetic couplings; Néel temperature; chemical pressure

Citation: Lafargue-Dit-Hauret, W.; Rocquefelte, X. Influence of the Chemical Pressure on the Magnetic Properties of the Mixed Anion Cuprates Cu_2OX_2 (X = Cl, Br, I). *Computation* **2022**, *10*, 73. https://doi.org/10.3390/computation10050073

Academic Editor: Henry Chermette

Received: 7 April 2022
Accepted: 24 April 2022
Published: 12 May 2022

1. Introduction

The design of multiferroics (MF) in which magnetic and ferroelectric orders are coupled is one of the hottest current topics in materials science [1]. These compounds appear as a fantastic playground to deeply investigate the origin and the interactions of the related ferroic properties and to design materials with improved or novel properties. Such multi-functional materials are also extremely appealing for the development of spintronic devices. For example, the control of a magnetic order by an electric field is targeted for several applications ranging from magnetic sensors to memory technologies. At the present time, very few MF compounds exhibit such properties at room temperature (RT), which dramatically limits potential industrial interests. In that context, we embarked on the quest for discovering high-temperature range MF materials, which ideally also show strong electric polarization.

Among the prospective strategies to tune MF stability domain(s) is the application of an hydrostatic (physical) pressure [2]. For instance, in 2013 [3], we predicted theoretically that under high pressure values of about 20 GPa, CuO would become MF at RT. This prediction has been confirmed through dielectric constants measurements up to 7 GPa in 2021 [4] and more recently by neutron diffraction up to 18.5 GPa [5]. An alternative route is to apply a chemical pressure through chemical substitutions, leading to create internal constraints. For instance, the two multiferroic compounds $CuCl_2$ [6] and $CuBr_2$ [7] are characterized by Néel temperatures of 23.9 K and 73.5 K, respectively. Such an increase of T_N is the direct consequence of the chemical substitution of Cl by Br.

Herein, we propose to study the mixed anion system Cu_2OX_2 (with X = Cl, Br, I). It derives from the CuO compound in which half of the O^{2-} ions have been replaced by two X^- ions. Magnetic measurements performed on Cu_2OCl_2 evidenced an antiferromagnetic order with a Néel temperature of ∼70 K [8,9], which was firstly attributed to an all-in-all-out arrangement of magnetic moments carried by Cu^{2+} centers forming a pyrochlore-like lattice [10]. Then, powder neutron diffraction analyses [11] revealed an incommensurate magnetic order, with a propagation vector $\vec{q} = [0.827(7), 0, 0]$ and concomitant with a ferroelectric phase. It has also been evidenced that the incommensurate magnetic structure induces a spin–phonon coupling similar to the ones observed in perovskite compounds [12]. In 2019, two contradictory neutron-scattering investigations were published. In the first investigation [13], the spin-driven nature of the multiferroicity of Cu_2OCl_2 was demonstrated, leading to the proposition of a cycloidal non-collinear magnetic order with competing magnetic exchange couplings and driven by an inverse Dzyaloshinskii–Moriya mechanism. In the second article [14], the authors claimed the simultaneous existence, at low temperature, of a collinear antiferromagnetic order and an antiferroelectric phase resulting from a Cl→O charge transfer.

In terms of J magnetic exchange values, only one experimental estimation from magnetic susceptibilty [8] has been proposed, one conference's abstract gave contradicting values deduced from Density Functional Theory (DFT) calculations [15] without providing any details, and one last article [13] focused on the sign of J couplings by studying Wannier functions with DFT. The present study aims to clarify the understanding of the magnetic interactions in Cu_2OCl_2 by doing DFT calculations at ambient pressure but also under chemical pressure, by predicting the magnetic properties of Cu_2OBr_2 and Cu_2OI_2, for the very first time.

2. Materials and Methods

Geometry optimizations on the isostructural Cu_2OX_2 (X = Cl, Br, I) systems were performed within the Density Functional Theory (DFT) framework using the PAW method, as implemented in the VASP code [16–18]. Valence electrons were treated using the following electronic configurations for the different species: $3p^2 4s^2 3d^9$ for Cu, $3s^2 3p^5$ for Cl, $4s^2 4p^5$ for Br, $5s^2 5p^5$ for I and $2s^2 2p^4$ for O. The PBE approach was considered for the exchange–correlation functional [19]. To improve the description of the electronic properties for Cu-3d orbitals, a Hubbard effective correction following Dudarev's scheme [20] was used. We previously showed that U_{eff} = 6.5 eV enables us to recover the experimental volume variation under hydrostatic pressure for the CuO compound [3]. Here, an identical value was chosen. Long-distance van der Waals interactions were taken into account by introducing the DFT-D3 correction proposed by Grimme et al. [21]. Spin-polarized simulations were done with a 5 × 4 × 4 Γ-centered k-mesh and a cutoff energy of 550 eV. The dynamical stability of all optimized structures was checked by computing the phonon modes with the finite-differences method for symmetrically non-equivalent displacements on a 2 × 1 × 1 supercell and a 2 × 4 × 4 Γ-centered k-mesh.

For each compound, the exchange couplings were estimated based on the optimized structures with the Wien2K code, using DFT within the FP-LAPW approach [22]. The PBE0 on-site functional was chosen for the treatment of the exchange correlation part in the lines of our previous works [3,4]. The RK_{max} parameter was set to 7. Muffin-Tin radii were fixed to 1.94, 2.10, 2.20 and 1.71 a_0 for Cu, Cl, Br, I and O species, respectively. The first Brillouin zone was sampled with 52–58 irreducible k-points. The magnetic interactions were extracted from a least-squares fitting procedure applied between the DFT energy related to a given collinear magnetic state and the energy of an Ising Hamiltonian used to describe the magnetic structure:

$$E_{Ising} = \sum_{i \neq j} S_i \cdot J_{ij} \cdot S_j \quad (1)$$

where S_i and S_j are the spins carried by the Cu_i and Cu_j centers, respectively. The J_{ij} parameter represents the magnetic exchange interactions between S_i and S_j. Hereafter, $J > 0$ indicates an antiferromagnetic (AFM) coupling, and $J < 0$ indicates a ferromagnetic (FM) coupling.

3. Results and Discussion

3.1. Crystal Structure of Cu_2OCl_2

The melanothallite Cu_2OCl_2 crystallizes in the orthorhombic space group *Fddd* with a = 7.4477 Å, b = 9.5989 Å, c = 9.6888 Å, V = 692.65 Å^3, and Z = 8 [11]. The structure shown in Figure 1a is characterized by one symmetrically non-equivalent Cu^{2+} site located in a strongly distorted octahedral environment due to a Jahn–Teller effect. It can be viewed as a CuO_2Cl_2 square-planar environment (also called plaquette), in which the bond lengths are d_{Cu-O} = 1.943 Å and d_{Cu-Cl} = 2.283 Å. Two longer bonds are formed with chlorine ions in apical positions with d_{Cu-Cl} = 3.123 Å. These CuO_2Cl_2 *plaquettes* are sharing edges to form ribbons which are inter-connected together by the oxygen ions in a three-dimensional network, which has many common features with the CuO atomic structure. For instance, both Cu_2OCl_2 and CuO [23–25] exhibit unusual thermal variations of lattice parameters due to the so-called hinge mechanism [26]. The ribbons are parallel to the [110] and $[\bar{1}10]$ directions. As shown in Figure 1b, another vision of the structure is a pyrochlore-like lattice where the tridimensional network is based on O-centered OCu_4 tetrahedra which are sharing corners. Here, the chlorine species are pointing toward the center of cavities.

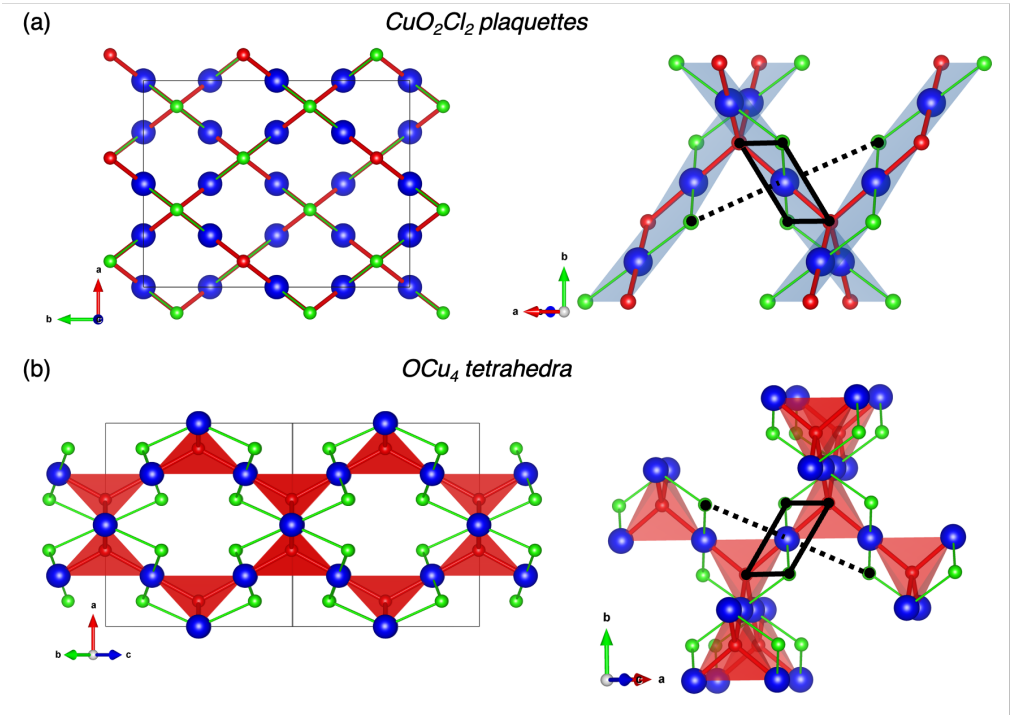

Figure 1. Crystallographic structure of Cu_2OCl_2 described by (**a**) Cu-centered CuO_2Cl_2 square planar environments and (**b**) O-centered OCu_4 tetrahedral environments. The blue, red and green spheres represent copper, oxygen and chlorine ions, respectively. Square planar and tetrahedral environments are evidenced in transparent blue and red, respectively. The CuO_2Cl_4 distorted octahedral environment is highlighted with black lines.

3.2. Geometry Optimization

Geometry relaxations have been performed at ambient pressure in order to validate our approach by comparing with the experimental data of Cu_2OCl_2 and to predict the atomic structure of Cu_2OBr_2 and Cu_2OI_2. The experimental Cu_2OCl_2 structure reported in Ref. [11] was used as an initial guess for all compounds. The main structural parameters

of the optimized geometries are summarized in Table 1, including the experimental data of Cu_2OCl_2.

Table 1. Optimized structural parameters of the Cu_2OX_2 compounds (X = Cl, Br, I) deduced from DFT+U calculations ($U_eff[Cu(3d)] = 6.5$ eV) and experimental data of Cu_2OCl_2 Ref. [11]. For Cu_2OCl_2, the deviation (in percentage) with respect to the experimental data is given in parentheses.

	Cu_2OCl_2 (Exp.)	**Cu_2OCl_2**	**Cu_2OBr_2**	**Cu_2OI_2**
a (Å)	7.4477	7.4675 (+0.3)	7.7203	8.1680
b (Å)	9.5989	9.6448 (+0.5)	9.9962	10.5578
c (Å)	9.6888	9.7337 (+0.5)	9.7661	10.1226
V (Å^3)	692.65	701.05 (+1.2)	753.69	872.93
z_X	0.3241	0.3237 (−0.1)	0.3138	0.3104
Cu-O (Å)	1.943	1.951 (+0.4)	1.996	2.094
Cu-X_{eq} (Å)	2.283	2.295 (+0.5)	2.408	2.543
Cu-X_{ap} (Å)	3.123	3.132 (+0.3)	3.214	3.391
Cu-O-Cu (°)	102.86	102.82 (0.0)	104.58	105.65
Cu-X_{eq}-Cu (°)	83.42	83.25 (−0.2)	81.93	82.01
hinge angle (°)	63.20	63.13 (−0.1)	62.42	62.10

Regarding Cu_2OCl_2, an excellent agreement is found between the experimental and the theoretical structures. The optimized lattice parameters deviate from the experimental ones by less than 0.5%. Considering the first neighbor's shell, the Cu-O, Cu-Cl_{eq} and Cu-Cl_{ap} bonds of the optimized geometry are 1.95, 2.30 and 3.13 Å, respectively (deviation smaller than 0.5%). Inside a ribbon, the Cu-O-Cu and Cu-Cl_{eq}-Cu bond angles are computed at 102.8° and 85.25° (less than 0.2% deviation), respectively. Finally, the hinge angle that corresponds to the Cu-O-Cu angle between two ribbons is 63.1° (0.1% deviation).

Focusing now on the new Cu_2OBr_2 compound, one may notice that the lattice parameters are larger than the optimized ones of Cu_2OCl_2, as expected from the larger atomic size of bromine. It leads to $a = 7.720$ Å (3.4% larger compared to Cu_2OCl_2), $b = 9.996$ Å (3.6% larger), $c = 9.766$ Å (0.3% larger), and $V = 753.69$ Å^3 (7.5% larger). This steric effect mainly affects a and b parameters, which are defining the directions of the ribbons. The optimized Cu-O, Cu-Br_{eq} and Cu-Br_{ap} bond lengths are 2.00, 2.41 and 3.21 Å, respectively. The angles within a ribbon, i.e., Cu-O-Cu and Cu-Br_{eq}-Cu, are about 2° larger and 1.3° smaller than in Cu_2OCl_2, respectively. The hinge angle appears slightly smaller than in Cu_2OCl_2 at 62.42°.

For the second new compound Cu_2OI_2, the lattice parameters are still increasing compared to the two former cases, following the chemical sense directed by the atomic radii ($r_{Cl} < r_{Br} < r_I$). In detail, we found a = 8.168 Å (9.4% larger compared to Cu_2OCl_2), b = 10.558 Å (9.5% larger), c = 10.123 Å (4.0% larger) and V = 872.93 Å^3 (24.5% larger). Once more, the significant variation of volume results from more important changes reported for a and b lattice parameters. Regarding the distorted CuO_2I_4 environment, the optimized Cu-O, Cu-I_{eq} and Cu-I_{ap} bond lengths are respectively measured at 2.09, 2.54 and 3.39 Å. Focusing on the ribbons, the Cu-O-Cu angle equals 105.7° (2.3° larger than in Cu_2OCl_2), while the Cu-I_{eq}-Cu angle is reduced to 82.0° (1.2% smaller).

No imaginary phonon frequencies were retrieved for both Cu_2OCl_2 and Cu_2OBr_2 systems. First, this result confirms that the present modeling reproduces properly both the atomic parameters and the dynamical stability of Cu_2OCl_2. Experimentally, the crystals are grown using the chemical vapor transport techniques with a stoichiometric mixture of CuO and $CuCl_2$ compounds [11]. Second, Cu_2OBr_2 is predicted to be dynamically stable. For Cu_2OI_2, one imaginary phonon frequency was calculated at $\sim 20i$ cm^{-1}, suggesting that such a phase does not exist. However, Cu_2OI_2 was kept in our investigation as a virtual compound allowing us to probe the chemical pressure effect.

3.3. Electronic Properties

Based on the optimized structures, the electronic properties were investigated using the Wien2K code. The projected density of states (pDOS) of the three Cu_2OX_2 systems are represented in Figure 2. The present PBE0 calculations lead to band gap values of 2.18 eV, 1.85 eV and 0.95 eV for X = Cl, Br and I, respectively, and rather similar pDOS. The valence band (VB) is based on the O-2*p*, Cl-3*p* (or Br-4*p* or I-5*p*) and Cu-3*d* states (from −7 to 0 eV with respect to E_F). While the top of the VB is mainly composed of O-2*p* states in Cu_2OCl_2, it is mainly based on Br-4*p* and I-5*p* states in Cu_2OBr_2 and Cu_2OI_2, respectively. Such a point is emphasized in Figure 3 by the electronic densities calculated in the energy range from −0.5 to 0 eV (with respect to E_F). The magnetically active orbital, i.e., the one carrying the magnetic moment, is the Cu-3$d_{x^2-y^2}$, as expected from the d^9 electronic configuration and the square planar environment. The calculated magnetic moment of copper is 0.6–0.7 μ_B in Cu_2OX_2, which is in good agreement with the available experimental data for Cu_2OCl_2. Indeed, the ordered magnetic moment was found to be 0.64(5) μ_B and 0.66(2) μ_B from powder and single-crystal neutron refinements, respectively [13].

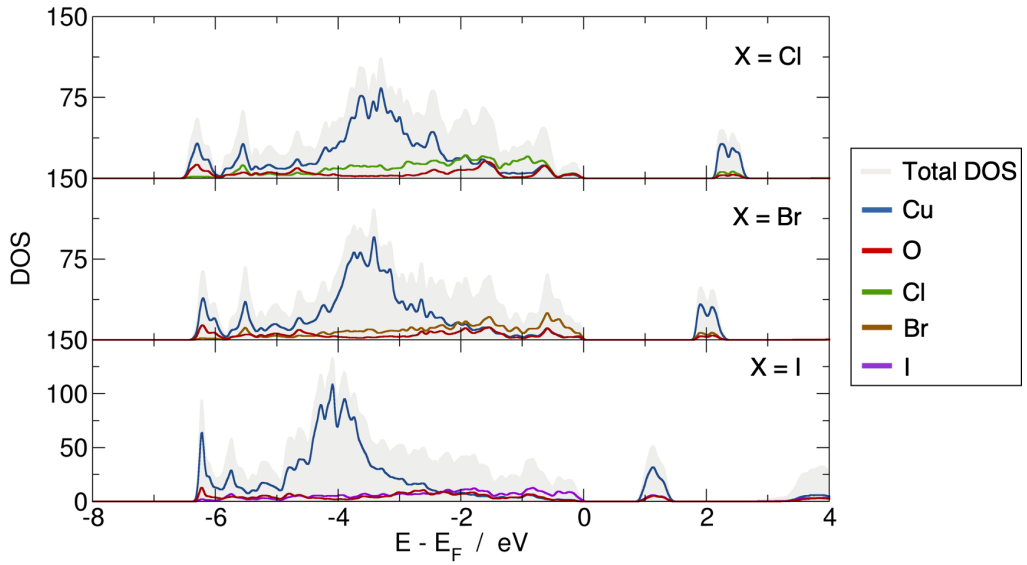

Figure 2. Total and projected densities of states for the Cu_2OX_2 compounds (X = Cl, Br, I) deduced from PBE0 on-site calculations on the ground-state AFM collinear order. Energies for pDOS are given with respect to E_F.

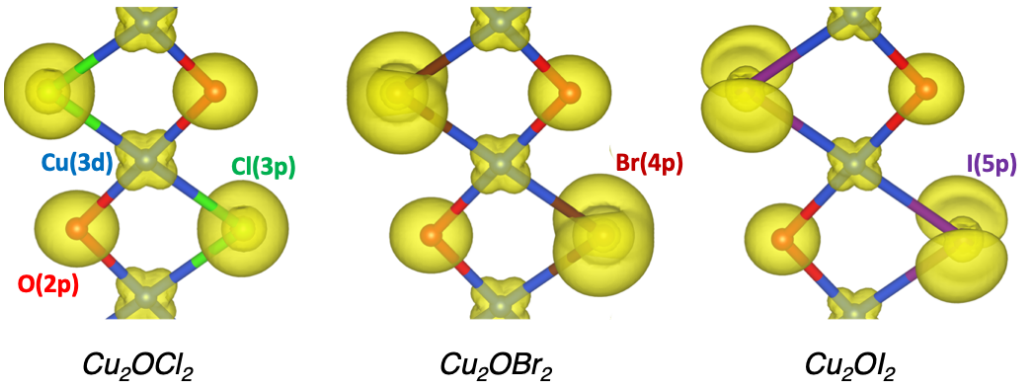

Figure 3. Electronic density corresponding to the top of the valence band (from −0.5 to 0 eV with respect to E_F) for the Cu_2OX_2 compounds (X = Cl, Br, I) deduced from PBE0 on-site calculations on the ground state AFM collinear order. Isovalue is set to 0.1 electron/Å^3. Blue, red, green, brown and violet spheres indicate Cu, O, Cl, Br and I atoms, respectively.

3.4. Magnetic Exchange Interactions

Magnetic susceptibiltity measurements on Cu_2OCl_2 provided a Néel temperature T_N of ∼70 K followed by a broad maximum at ∼140 K [8,9]. Many investigations were carried out to determine the nature of the magnetic order at lower temperatures, leading to several propositions such as an *all-in-all-out* model [10], an incommensurate spin spiral phase [11], an incommensurate spin cycloidal phase [13] and a collinear antiferromagnetic (AFM) phase [14]. However, only one of these experimental investigations proposed magnetic exchange coupling (J) values extracted from magnetic susceptibility fits [8], which are in disagreement with the reported J values estimated from DFT calculations [15]. However, these latter values were found in a conference abstract and no related publication is available, to our knowledge.

Based on the optimized geometries, we have thus calculated the J exchange values using PBE0 on-site functional as we did for CuO [3,4]. Examining the atomic structure leads to defining four magnetic interactions depicted in Figure 4 for both ribbons- and pyrochlore-like lattices. The related d_{Cu-Cu} bond lengths and Cu-O-Cu angles are specified in Table 2 for Cu_2OCl_2, Cu_2OBr_2 and Cu_2OI_2. More specifically, considering the ribbons-like structure, we targeted two intra-ribbon (J_1 and J_4) and two inter-ribbon (J_2 and J_3) couplings. It should be noticed that among these four interactions, only J_4 is based on a super-superexchange (SSE) path, i.e., the magnetic moments are mediated through an orbital overlap implying two ligand atoms (namely Cu-L-L-Cu, with L = O, Cl, Br or I), the others being based on a superexchange (SE) path implying only one ligand atom (namely Cu-L-Cu, with L = O, Cl, Br or I).

The J couplings were estimated using the *mapping analysis* procedure. The strategy consists of (1) determining the DFT energies of a set of magnetic states, (2) defining the related energy expressions in terms of J parameters using an Ising Hamiltonian, and (3) refining the J parameters on top of the DFT results using a least squares method. One may underline that the accuracy of such an approach strongly depends on the size and the quality of the set of magnetic states [27]. In our case, eight collinear magnetic structures were selected to obtain four J values. The results are summarized in Table 3.

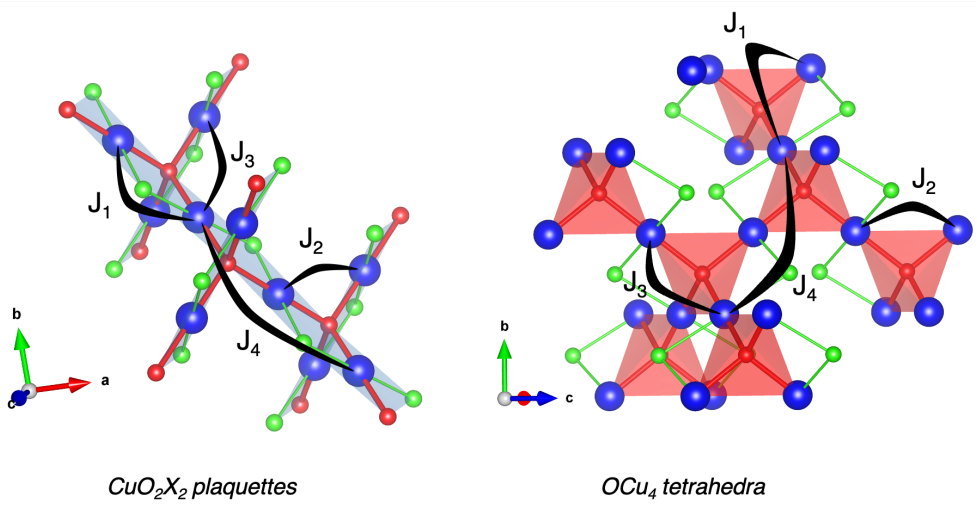

Figure 4. Representation of J exchange couplings between copper sites in both CuO_2X_2- and OCu_4-based frameworks. Cu, O and X atoms are depicted by blue, red and green spheres, respectively. CuO_2X_2 *plaquettes* and OCu_4 tetrahedra are shown in transparent blue and red, respectively.

Table 2. Geometrical parameters related to the four magnetic couplings for the Cu_2OX_2 compounds (X = Cl, Br, I) deduced from DFT+U relaxation ($U_eff[Cu(3d)] = 6.5$ eV). The experimental data of Cu_2OCl_2 taken from Ref. [11] are given in parentheses.

		J_1	J_2	J_3	J_4
Cu_2OCl_2	Cu-Cu (Å)	3.049 (3.037)	3.067 (3.055)	3.426 (3.410)	6.099 (6.075)
	Cu-O-Cu (°)	102.82 (102.86)	103.65 (103.70)	122.82 (122.72)	- -
Cu_2OBr_2	Cu-Cu (Å)	3.158	3.112	3.494	6.315
	Cu-O-Cu (°)	104.58	102.47	122.16	-
Cu_2OI_2	Cu-Cu (Å)	3.337	3.252	3.657	6.674
	Cu-O-Cu (°)	105.65	101.87	121.64	-

Table 3. Magnetic exchange interactions (in meV) calculated at the PBE0 on-site level for the Cu_2OX_2 compounds (X = Cl, Br, I). The available experimental and theoretical data are given for comparison. $J > 0$ indicates an AFM coupling, and $J < 0$ indicates an FM coupling.

		J_1	J_2	J_3	J_4
Cu_2OCl_2	This work	−14.0	−2.2	19.1	8.7
	Theo. [15]	−15.5	19.0 [1]		8.6
	Exp. [8]	9.7 [2]	9.3 [2]		-
Cu_2OBr_2	This work	−13.1	1.9	25.2	9.2
Cu_2OI_2	This work	−8.1	24.2	41.0	15.1

[1] This value has been defined as an interchain coupling without giving more details. It could be alternatively J_2, J_3 or a combined effective value. [2] These two parameters correspond to mean field estimation of $J_{intra-ribbon} = J_1$ and $J_{inter-ribbon} = J_2 + J_3$.

Before discussing our results, let us on comment the experimental values extracted by Okabe et al. [8] considering the ribbons-like picture. They considered two effective J parameters which were found to be both AFM and very close to each other, i.e., J_{intra} = 9.7 meV and J_{inter} = 9.3 meV, thus leading to strong magnetic frustrations. These mean field values can be compared to our J parameters considering that $J_{intra} = J_1 + J_4$ and $J_{inter} = J_2 + J_3$. It leads to DFT effective intra- and inter-ribbon couplings, which are respectively FM and AFM, i.e., J_{intra} = −5.3 meV and J_{inter} = 16.8 meV, in disagreement with Okabe et al. [8]. In contrast, in Ref. [15], three DFT J values have been proposed, i.e., two intra-ribbon (J_1 = −15.5 meV and J_4 = 8.6 meV) and one inter-ribbon ($J_{inter} = J_2 + J_3$ = 19.0 meV), which are in good agreement with our values, i.e., J_1 = −14.0 meV and J_4 = 8.7 meV for the intra-ribbon interactions and J_2 = −2.2 meV and J_3 = 19.1 meV for the inter-ribbon ones.

In other words, the present calculations evidenced that the ribbons are mainly FM ordered due to the first-neighbor (SE) interaction J_1, and the spins are frustrated due to the AFM second-neighbor (SSE) interaction J_4, which is 1.6 times smaller than J_1 in amplitude. Between the ribbons, the interaction is AFM due to J_3 (J_2 appears negligible). In the pyrochlore-like lattice, each OCu_4 tetrahedron is globally AFM with two up and two down magnetic centers, which further emphasizes the spin frustration character of the magnetic structure. The resulting most stable collinear magnetic order is depicted in Figure 5.

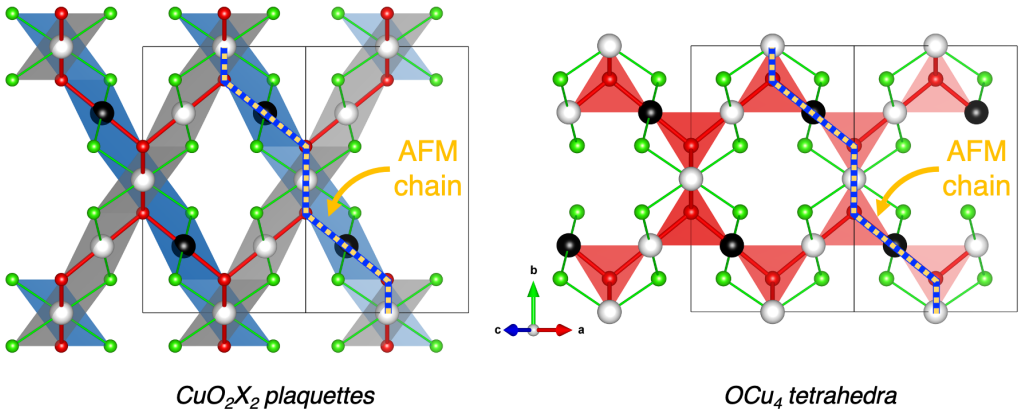

Figure 5. Schematic representation of the ground-state AFM collinear magnetic structure within the (**left**) ribbons- and (**right**) pyrochlore-like lattices. Black and white spheres indicate up and down spins carried by Cu sites, respectively. Red and green spheres represent oxygen and halogen species, respectively. The OCu_4 tetrahedral coordinations are represented in transparent red. The CuO_2X_2 *plaquettes* are shown in transparent blue and gray for an up or down spin carried by the central Cu, respectively. One AFM spin chain, formed by the $J = J_3$ coupling and considered within the quasi-1D AFM model, is evidenced by a yellow–blue dotted line.

A similar picture is obtained for Cu_2OBr_2 and Cu_2OI_2 compounds. Regarding the intra-ribbon interactions, one may notice that the FM J_1 coupling decreases to -13.1 meV and -8.1 meV, respectively, while the AFM J_4 coupling is enhanced to 9.2 meV and 15.1 meV, respectively. For the inter-ribbon interactions, the FM J_2 coupling becomes AFM at 1.9 meV for Cu_2OBr_2 and strongly increases up to 24.2 meV for Cu_2OI_2. J_3 stays the strongest (AFM) coupling and is increased to 25.2 meV and 41.0 meV, respectively. The larger values for J_3 cannot be explained only based on geometrical arguments. Indeed, the related Cu-O bond length and Cu-O-Cu angle, respectively, increases and decreases, when Cl is substituted by Br or I. It is the signature that the halogen element indirectly participates in this interaction by setting the size and the shape of the magnetic orbital due to the nephelauxetic effect, which increases in the series $Cl^- < Br^- < I^-$, leading to an expansion of the copper $3d$ orbitals and thus larger interactions. Figure 6 shows that the spin densities of the three compounds are quite similar, with spin-up densities (in yellow) along the FM J_1 coupling for both copper and halogen elements involved in this interaction. For oxygen atoms, which are also involved in the AFM couplings (J_3 and J_4), two lobes are found with one up- and one down-spin densities in yellow and cyan, respectively. These observations have a direct consequence on the magnetic moments carried by the ligands, which are 0.11, 0.10, 0.08 and 0.00 μ_B for Cl, Br, I and O, respectively. Indeed, the magnetic moment of the oxygen is null due to its participation in AFM couplings.

To go further, we focused more deeply on the magnetically active orbital, i.e., Cu-$3d_{x^2-y^2}$, and its interaction with the surrounding ligands. The spin-polarized pDOS of Cu-$3d_{x^2-y^2}$, O-$2p$ and Cl-$3p$ states of one *plaquette* are given in Figure 7a for Cu_2OCl_2. It appears that the occupied Cu-$3d_{x^2-y^2}$ states are mainly positioned within the energy range from -7 to -5 eV (highlighted by the gray dotted line rectangle). The electronic charge density (ρ) and spin density related to this energy window are shown in Figure 7b,c, respectively. First of all, from the analysis of both pDOS and ρ, it appears that the Cu-$3d_{x^2-y^2}$ orbital interaction is larger with O-$2p$ than Cl-$3p$ states. It confirms that the magnetic moment of the magnetically active orbital is mainly mediated by oxygen atoms and thus justifies that the largest coupling is along a Cu-O-Cu superexchange path. In addition, the up- and down-pDOS of O-$2p$ states are perfectly symmetric, leading to a net magnetic moment of zero. Similarly, the spin-density around oxygen is constituted of two equivalent lobes with opposite spins (as previously discussed). Looking in more detail, Figure 7c evidenced the pivotal role of oxygen that connects two ribbons (with opposite spins), which are nearly perpendicular. To summarize the results of the present analysis, the magnetically active

orbital results from an overlap of Cu-3$d_{x^2-y^2}$ with O-2p and to a less extent with Cl-3p states in Cu_2OCl_2. One may notice that in this energy range, the pDOS of the magnetically active orbital is constituted by two peaks: (1) the lower in energy originating from the Cu-O interaction, while (2) the higher in energy is associated to the Cu-Cl interaction. A similar picture can be retrieved for Cu_2OBr_2 and Cu_2OI_2, except that the first peak (Cu-O interaction) increases and the second peak (Cu-X interaction) decreases (see Figure 2). This observation explains the enhancement of J_3 from Cu_2OCl_2 to Cu_2OBr_2 and to Cu_2OI_2.

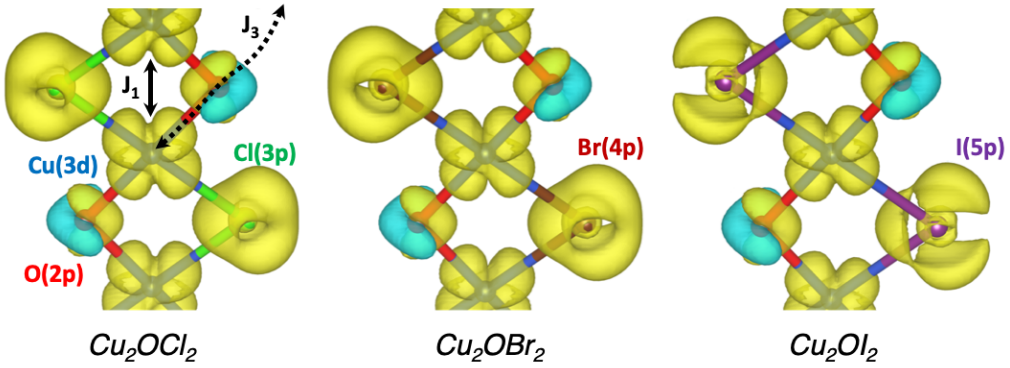

Figure 6. Spin density for the AFM ground state of Cu_2OCl_2, Cu_2OBr_2 and Cu_2OI_2. The isovalue is set to 0.017 electron/Å^3, up and down regions of the spin density are evidenced in transparent yellow and cyan, respectively. Blue, red, green, brown and violet spheres indicate Cu, O, Cl, Br and I atoms, respectively. The FM J_1 and AFM J_3 couplings are indicated.

Interestingly, these three systems can be compared to their parent compound CuO, for which the atomic and magnetic structures are described using different descriptors. While the atomic structure can be viewed as based on ribbons of edge-sharing CuO_4 *plaquettes*, the magnetic order is mainly governed by AFM spin chains of corner-sharing CuO_4 *plaquettes*. Here also, it appears that the strongest magnetic coupling, i.e., J_3, is at the origin of AFM spin chains of corner-sharing CuO_2X_2 *plaquettes*, highlighted by a yellow–blue dotted line in Figure 5. The presence of such AFM spin chains can be more clearly seen and understood in the OCu_4-based vision, where these AFM spin chains propagate along tetrahedra.

As we did previously for CuO [3,4], we can thus estimate T_N based on the random phase approximation model of a quasi-1D AFM Heisenberg cubic lattice [28]:

$$J' = \frac{T_N}{4c\sqrt{\ln(\alpha J/T_N) + 0.5\ln(\ln(\alpha J/T_N))}} \quad (2)$$

where $\alpha = 2.6$ and $c = 0.233$ are numerical parameters, J' is an effective inter-chain coupling and J is the intra-chain coupling. In the present case, half of the spin chains are 90° rotated, leading to half as many inter-chain couplings. The resulting ground-state expression is $E_{GS}(model) = J + J'$, instead of $E_{GS}(model) = J + 2J'$ in the CuO model where all chains are oriented in the same direction. Such an expression has to be compared to the collinear ground-state (Figure 5) energy defined as:

$$E_{GS} = J_3 - J_1 + J_2 - J_4 \quad (3)$$

Thus, one may define:

$$J = J_3 \quad (4)$$

$$J' = -J_1 + J_2 - J_4 \quad (5)$$

Using the aforementioned J values and the original c and α parameters, we obtain T_N = 65, 111 and 294 K for Cu_2OCl_2, Cu_2OBr_2 and Cu_2OI_2, respectively (see Figure 8). Experimentally, T_N ∼70 K for Cu_2OCl_2. Such a good agreement validates the present magnetic model, which consists of considering AFM spin chains based on $J = J_3$ interacting through an effective coupling defined as $J' = -J_1 + J_2 - J_4$. It should be noticed that if we use the refined value for CuO c = 0.284 [3], we obtain T_N = 77, 131 and 344 K for Cu_2OCl_2, Cu_2OBr_2 and Cu_2OI_2, respectively (see Figure 8). The agreement for Cu_2OCl_2 is still very good with the experiment, and whatever the c value is, we predict a significant increase of T_N when Cl is replaced by either Br or I in the compound. A similar trend has been reported experimentally for $CuCl_2$ and $CuBr_2$ [6,7], for which T_N = 23.9 and 77 K, respectively.

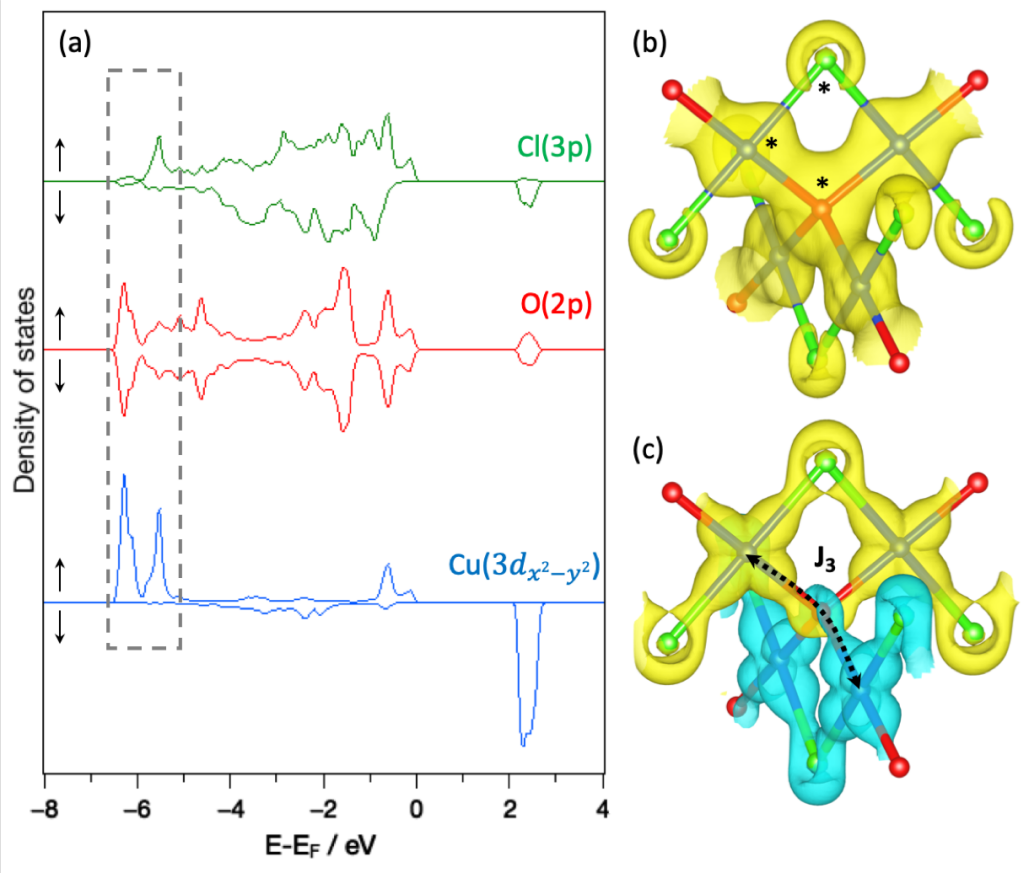

Figure 7. (**a**) Spin-polarized projected density of states (pDOS) of one *plaquette* in Cu_2OCl_2. The energy window of Cu-3$d_{x^2-y^2}$ occupied states is evidenced by a gray dotted rectangle on the pDOS. The (**b**) electronic charge density and (**c**) the spin density calculated in this energy range are also displayed. The atoms considered for the pDOS are shown by black stars on the electronic charge density. Up and down spin channels of the pDOS are evidenced by ↑ and ↓, respectively. Isovalues are set to 0.1 and 0.017 electron/Å^3 for electronic charge density and the spin density, respectively. Up and down regions of the spin density are highlighted in transparent yellow and cyan, respectively. Blue, red and green spheres indicate Cu, O and Cl atoms, respectively.

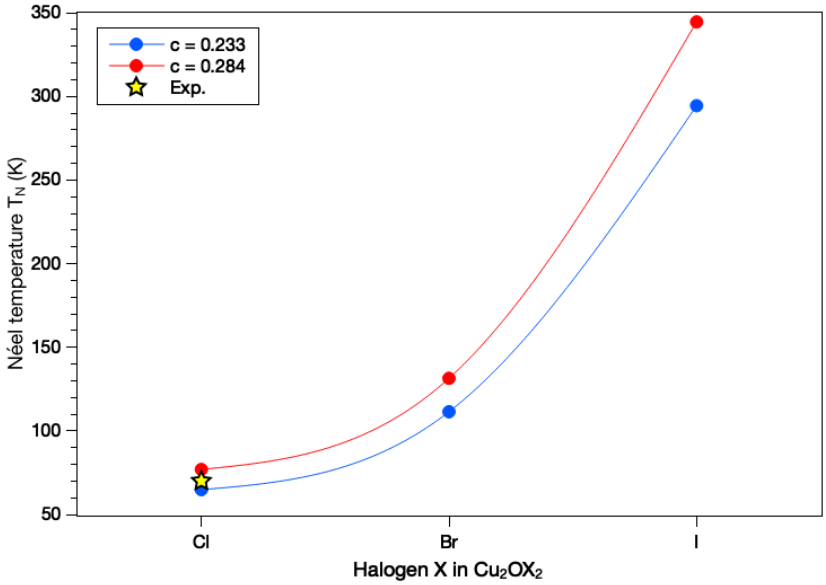

Figure 8. Estimation of the T_N Néel temperature depending on the nature of halogen species and considering two sets of parameters for the magnetic model presented in Equation (2): (1, in blue) α = 2.6 and c = 0.233, and (2, in red) α = 2.6 and c = 0.284. The experimental value for Cu_2OCl_2 is represented by a yellow star.

4. Conclusions

In summary, we have investigated the magnetic properties of Cu_2OX_2 (X = Cl, Br, I) systems based on first-principles calculations. The atomic structure of Cu_2OX_2 can be viewed either as based on ribbons of CuO_2X_2 edge-sharing *plaquettes* or as a pyrochlore-like lattice constituted of OCu_4 corner-sharing tetrahedra. The present study shows that the magnetic order is governed by AFM spin chains of CuO_2X_2 corner-sharing *plaquettes*, which defines an AFM intra-chain coupling $J = J_3$. These spin chains interact with each other through three inter-chain couplings, which leads to an effective interaction $J' = -J_1 + J_2 - J_4$. Using these two parameters J and J' in an analytical expression for a quasi-1D AFM Heisenberg system, one may recover the Néel temperature of the known multiferroic compound Cu_2OCl_2 at $T_N = 70$ K. We also predict that Cu_2OBr_2 could be a stable phase and is expected to have a larger T_N value, which is evaluated to be about 120 K. Using chemical pressure to enhance T_N is thus an effective and appealing technique to design new mixed anion compounds in order to reach RT operating MF. Ongoing investigations in our group consist of combining chemical and physical pressures to reach this goal.

Author Contributions: Investigation, W.L.-D.-H.; supervision, X.R.; formal analysis, writing—original draft preparation, review and editing, W.L.-D.-H., X.R. All authors have read and agreed to the published version of the manuscript.

Funding: Research funded by Agence Nationale de la Recherche (ANR-19-CE08-0013).

Institutional Review Board Statement: Not applicable.

Informed Consent Statement: Not applicable.

Data Availability Statement: The data presented in this study are available in insert article.

Acknowledgments: The theoretical work was granted access to the HPC resources of TGCC/CINES /IDRIS under Allocation No. 2019-A0050907682 made by GENCI. The authors also acknowledge the CCIPL (Centre de Calcul Intensif des Pays de la Loire) for computational resources. Crystal structures were represented using the VESTA software [29].

Conflicts of Interest: The authors declare no conflict of interest.

References

1. Fiebig, M.; Lottermoser, T.; Meier, D.; Trassin, M. The evolution of multiferroics. *Nat. Rev. Mater.* **2016**, *1*, 16046. [CrossRef]
2. Gilioli, E.; Ehm, L. High pressure and multiferroics materials: A happy marriage. *Int. Union Crystallogr. J.* **2014**, *1*, 590–603. [CrossRef] [PubMed]
3. Rocquefelte, X.; Schwarz, K.; Blaha, P.; Kumar, S.; van den Brink, J. Room-temperature spin-spiral multiferroicity in high-pressure cupric oxide. *Nat. Commun.* **2013**, *4*, 2511. [CrossRef] [PubMed]
4. Lafargue-Dit-Hauret, W.; Braithwaite, D.; Huxley, A.D.; Kimura, T.; Saúl, A.; Rocquefelte, X. Potential room-temperature multiferroicity in cupric oxide under high pressure. *Phys. Rev. B* **2021**, *103*, 214432. [CrossRef]
5. Manuel, P. Private communication. 2022.
6. Banks, M.G.; Kremer, R.K.; Hoch, C.; Simon, A.; Ouladdiaf, B.; Broto, J.M.; Rakoto, H.; Lee, C.; Whangbo, M.H. Magnetic ordering in the frustrated Heisenberg chain system cupric chloride $CuCl_2$. *Phys. Rev. B* **2009**, *80*, 024404. [CrossRef]
7. Zhao, L.; Hung, T.L.; Li, C.C.; Chen, Y.Y.; Wu, M.K.; Kremer, R.K.; Banks, M.G.; Simon, A.; Whangbo, M.H.; Lee, C.; et al. $CuBr_2$—A New Multiferroic Material with High Critical Temperature. *Adv. Mater.* **2012**, *24*, 2469–2473. [CrossRef]
8. Okabe, H.; Suzuki, K.; Kawashima, K.; Muranaka, T.; Akimitsu, J. New Pyrochlore-like Compound Cu_2OCl_2 with S = 1/2. *J. Phys. Soc. Jpn.* **2006**, *75*, 123705. [CrossRef]
9. Kawashima, K.; Okabe, H.; Suzuki, K.; Kuroiwa, S.; Akimitsu, J.; Sato, K.H.; Koda, A.; Kadono, R. Antiferromagnetic ordering in Cu_2OCl_2 studied by the muon spin rotation/relaxation technique. *J. Phys. Condens. Matter* **2007**, *19*, 145275. [CrossRef]
10. Nishiyama, M.; Oyamada, A.; Itou, T.; Maegawa, S.; Okabe, H.; Akimitsu, J. NMR study of pyrochlore lattice antiferromagnet, melanothallite Cu_2OCl_2. *J. Phys. Conf. Ser.* **2011**, *320*, 012030. [CrossRef]
11. Zhao, L.; Fernández-Díaz, M.T.; Tjeng, L.H.; Komarek, A.C. Oxyhalides: A new class of high-T_c multiferroic materials. *Sci. Adv.* **2016**, *2*, e1600353. [CrossRef]
12. Araújo, B.S.; Arévalo-López, A.M.; Attfield, J.P.; Paschoal, C.W.A.; Ayala, A.P. Spin-phonon coupling in melanothallite Cu_2OCl_2. *Appl. Phys. Lett.* **2018**, *113*, 222901. [CrossRef]
13. Guo, H.; Zhao, L.; Schmidt, W.; Fernández-Díaz, M.T.; Becker, C.; Melendez-Sans, A.; Peng, W.; Zbiri, M.; Hansmann, P.; Komarek, A.C. Multiferroic properties of melanothallite Cu_2OCl_2. *Phys. Rev. Mater.* **2019**, *3*, 124405. [CrossRef]
14. Wu, H.C.; Yuan, J.K.; Chandrasekhar, K.D.; Lee, C.H.; Li, W.H.; Wang, C.W.; Chen, J.M.; Lin, J.Y.; Berger, H.; Yen, T.W.; et al. Observation of charge–transfer–driven antiferroelectricity in 3d-pyrochlore multiferroic Cu_2OCl_2. *Mater. Today Phys.* **2019**, *8*, 34–42. [CrossRef]
15. Tsirlin, A.A.; Janson, O.; Rosner, H. *Electronic Structure and Magnetic Properties of Melanothallite (Cu_2OCl_2), a Gateway to Understanding Copper Oxychlorides*; Russian Mineralogical Society: Kirovsk, Russia, 2010; Volume 1, p. 61.
16. Kresse, G.; Furthmüller, J. Efficiency of ab-initio total energy calculations for metals and semiconductors using a plane-wave basis set. *Comput. Mater. Sci.* **1996**, *6*, 15–50. [CrossRef]
17. Kresse, G.; Furthmüller, J. Efficient iterative schemes for ab initio total-energy calculations using a plane-wave basis set. *Phys. Rev. B* **1996**, *54*, 11169–11186. [CrossRef]
18. Kresse, G.; Joubert, D. From ultrasoft pseudopotentials to the projector augmented-wave method. *Phys. Rev. B* **1999**, *59*, 1758–1775. [CrossRef]
19. Perdew, J.P.; Burke, K.; Ernzerhof, M. Generalized Gradient Approximation Made Simple. *Phys. Rev. Lett.* **1996**, *77*, 3865–3868. [CrossRef]
20. Dudarev, S.L.; Botton, G.A.; Savrasov, S.Y.; Humphreys, C.J.; Sutton, A.P. Electron-energy-loss spectra and the structural stability of nickel oxide: An LSDA+U study. *Phys. Rev. B* **1998**, *57*, 1505–1509. [CrossRef]
21. Grimme, S.; Antony, J.; Ehrlich, S.; Krieg, H. A consistent and accurate ab initio parametrization of density functional dispersion correction (DFT-D) for the 94 elements H-Pu. *J. Chem. Phys.* **2010**, *132*, 154104. [CrossRef]
22. Blaha, P.; Schwarz, K.; Madsen, G.K.H.; Kvasnicka, D.; Luitz, J.; Laskowsk, R.; Tran, F.; Marks, L.; Marks, L. *WIEN2k: An Augmented Plane Wave Plus Local Orbitals Program for Calculating Crystal Properties*; Vienna University of Technology Institute of Materials Chemistry Getreidemarkt 9/165-TC A-1060: Vienna, Austria, 2019. ISBN 3-9501031-1-2.
23. Krivovichev, S.V.; Filatov, S.K.; Burns, P.C. The cuprite-like framework of OCu_4 tetrahedra in the crystal structure of synthetic melanothallite, Cu_2OCl_2, and its negative thermal expansion. *Can. Mineral.* **2002**, *40*, 1185–1190. [CrossRef]
24. Filatov, S.K.; Bubnova, R.S. The nature of special points on unit cell parameters temperature dependences for crystal substances. In *Tenth European Powder Diffraction Conference: Geneva, Switzerland, 1–4 September 2006*; Für Kristallographie, D.G., Ed.; Number 26; Oldenbourg Wissenschaftsverlag: Munchen, Germany, 2007; pp. 447–452.
25. Zheng, X.G.; Kubozono, H.; Yamada, H.; Kato, K.; Ishiwata, Y.; Xu, C.N. Giant negative thermal expansion in magnetic nanocrystals. *Nat. Nanotechnol.* **2008**, *3*, 724–726. [CrossRef] [PubMed]
26. Sleight, A.W. Compounds That Contract on Heating. *Inorg. Chem.* **1998**, *37*, 2854–2860. [CrossRef]
27. Rocquefelte, X.; Schwarz, K.; Blaha, P. Comment on High-T_c Ferroelectricity Emerging from Magnetic Degeneracy in Cupric Oxide. *Phys. Rev. Lett.* **2011**, *107*, 239701. [CrossRef] [PubMed]
28. Yasuda, C.; Todo, S.; Hukushima, K.; Alet, F.; Keller, M.; Troyer, M.; Takayama, H. Néel Temperature of Quasi-Low-Dimensional Heisenberg Antiferromagnets. *Phys. Rev. Lett.* **2005**, *94*, 217201. [CrossRef]
29. Momma, K.; Izumi, F. VESTA 3 for three-dimensional visualization of crystal, volumetric and morphology data. *J. Appl. Crystallogr.* **2011**, *44*, 1272–1276. [CrossRef]